Chin. Geogra. Sci. 2022 Vol. 32 No. 6 pp. 1083−1098
https://doi.org/10.1007/s11769-022-1318-9

Springer Science Press
www.springerlink.com/content/1002-0063

Application of Spatially Distributed Calibrated Hydrological Model in Evapotranspiration Simulation of Three Gorges Reservoir Area of China: A Case Study in the Madu River Basin

CHEN Junhong[1, 2], ZHANG Lihua[1, 2], CHEN Peipei[1, 2], MA Yongming[3]

(1. *School of Geography and Information Engineering*, *China University of Geosciences*, *Wuhan* 430074, *China*; 2. *Hubei Key Laboratory of Critical Zone Evolution*, *School of Geography and Information Engineering*, *China University of Geosciences*, *Wuhan* 430074, *China*; 3. *School of Geography and Tourism*, *Zhaotong University*, *Zhaotong*, 657000, *China*)

Abstract: Evapotranspiration (ET) is the key to the water cycle process and an important factor for studying near-surface water and heat balance. Accurately estimating ET is significant for hydrology, meteorology, ecology, agriculture, *etc*.. This paper simulates ET in the Madu River Basin of Three Gorges Reservoir Area of China during 2009−2018 based on the Soil and Water Assessment Tool (SWAT) model, which was calibrated and validated using the MODIS (Moderate-resolution Imaging Spectroradiometer)/Terra Net ET 8-Day L4 Global 500 m SIN Grid (MOD16A2) dataset and measured ET. Two calibration strategies (lumped calibration (LC) and spatially distributed calibration (SDC)) were used. The basin was divided into 34 sub-basins, and the coefficient of determination (R^2) and Nash-Sutcliffe efficiency coefficient (*NSE*) of each sub-basin were greater than 0.6 in both the calibration and validation periods. The R^2 and *NSE* were higher in the validation period than those in the calibration period. Compared with the measured ET, the accuracy of the model on the daily scale is: R^2= 0.704 and *NSE* = 0.759 (SDC results). The model simulation accuracy of LC and SDC for the sub-basin scale was R^2 = 0.857, R^2 = 0.862 (monthly) and R^2 = 0.227, R^2 = 0.404 (annually), respectively; for the whole basin scale was R^2 = 0.902, R^2 = 0.900 (monthly) and R^2 = 0.507 and R^2 = 0.519 (annually), respectively. The model performed acceptably, and SDC performed the best, indicating that remote sensing data can be used for SWAT model calibration. During 2009−2018, ET generally increased in the Madu River Basin (SDC results, 7.21 mm/yr), with a multiyear average value of 734.37 mm/yr. The annual ET change rate for the sub-basin was relatively low upstream and downstream. The linear correlation analysis between ET and meteorological factors shows that on the monthly scale, precipitation, solar radiation and daily maximum and minimum temperature were significantly correlated with ET; annually, solar radiation and wind speed had a moderate correlation with ET. The correlation between maximum temperature and ET is best on the monthly scale (Pearson correlation coefficient R = 0.945), which may means that the increasing ET originating from increasing temperature (global warming). However, the sub-basins near Shennongjia Nature Reserve that are in upstream have a negative ET change rate, which means that ET decreases in these sub-basins, indicating that the 'Evaporation Paradox' exists in these sub-basins. This study explored the potential of remote-sensing-based ET data for hydrological model calibration and provides a decision-making reference for water resource management in the Madu River Basin.

Keywords: soil and water assessment tool; distributed simulation for evapotranspiration; model calibration; remote sensing evapotranspiration products; Madu River Basin

Citation: CHEN Junhong, ZHANG Lihua, CHEN Peipei, MA Yongming, 2022. Application of Spatially Distributed Calibrated Hydrological Model in Evapotranspiration Simulation of Three Gorges Reservoir Area of China: A Case Study in the Madu River Basin. *Chinese Geographical Science*, 32(6): 1083−1098. https://doi.org/10.1007/s11769-022-1318-9

Received date: 2022-03-02; accepted date: 2022-06-07

Foundation item: Under the auspices of National Natural Science Foundation of China (No. 42271167), Open Fund of Hubei Key Laboratory of Critical Zone Evolution (No. CZE2022F03)

Corresponding author: ZHANG Lihua, E-mail address: zhanglihua@cug.edu.cn

1 Introduction

The coupling of basin-scale ecological and hydrological processes has attracted the attention of researchers (Newman et al., 2006), and physically-based hydrological models use variables and mathematical equations to model and calculate the interaction of climate-vegetation-hydrology processes to help us to understand various physical processes that occur in the real world. Thus, these models have become an important tool for quantitatively estimating water distribution in various environmental areas (Akoko et al., 2021). It is very important to calibrate and validate hydrological models before using them for making predictions and decisions, however, due to intensive human actions and climate change, the calibration of physically-based water balance models has become very challenging (Becker et al., 2019). Calibrations are usually performed with process-based variables. One variable of the hydrological processes that is closely related to water distribution is evapotranspiration (ET). As an important component of the terrestrial water cycle, ET links the terrestrial hydrological, energy, and carbon cycles. Accurately estimating regional ET is crucial for a wide range of research in hydrology, climate, crop yield forecasting, and drought monitoring (Zhang et al.,2010; Wu et al., 2020; Jepsen et al., 2021; Zhang et al., 2021; Zhuang et al., 2021). However, the estimation of ET is one of the most difficult components in the water cycle to estimate accurately due to the heterogeneity of the land surface and many other factors (Mu et al., 2007). There are some in situ measuring methods, such as weighing lysimeters (Howell et al., 1991), the Bowen ratio (Bowen, 1926), eddy covariance (Dyer, 1961), heat-pulse sensors and sap flow gauges (Wang et al., 2021), that can obtain the actual ET value. However, with these methods, it is inherently difficult to measure and predict ET at large spatial scales continuously over long time periods (Zeng et al., 2012). Eddy covariance is a relatively popular method for both actual ET measurements and ET estimation validation and is widely applied in global water and energy flux research (Zhang et al., 2010; Li et al., 2017; Jepsen et al., 2021; Zhuang et al., 2021), but it is discontinuous in the space-time domain and is difficult to measure at the regional scale (Zheng et al., 2020). More specifically, basins in many parts of the world are ungauged or poorly gauged (Sivapalan et al., 2003). For instance, the area examined in this study is located in the Three Gorges Reservoir area of China, which is a poorly gauged catchment (Bosshard and Zappa, 2008). In this case, remote sensing seems to have great potential for estimating ET. Many ET estimation approaches are driven by remote sensing data, such as the water mass balance equation (Zeng et al., 2012), energy balance model (Cui et al., 2021), machine learning model (Cui et al., 2021; Douna et al., 2021), surface energy balance algorithm (Bastiaanssen et al., 1998), and physically-based models (Immerzeel and Droogers, 2008; Wu et al., 2020; Jepsen et al., 2021). Moreover, there are some products of remotely sensed ET estimation, such as the MOD16 (MODIS (Moderate Resolution Imaging Spectroradiometer) Global Evapotranspiration Project) ET dataset (Mu et al., 2011) and GLEAM (The Global Land Evaporation Amsterdam Model) product (Xu et al., 2019). These ET products are currently available at a much finer spatial resolution than the effective spatial resolution of most stream gauges, the alternative and prevalent source of calibration data (Jepsen et al., 2021). Some studies have integrated remote sensing ET into hydrological model calibration (Gui et al., 2019; Herman et al., 2020; Jiang et al., 2020; Jin and Jin, 2020; Zhang et al., 2020c), and the SWAT (Soil and Water Assessment Tool) model, Xinanjiang model, SIMHYD (the Simple Lumped Conceptual Daily rainfall-runoff model) model, and VIC (Variable Infiltration Capacity) model are used in these studies. However, they all paid more attention to runoff and used runoff data in the calibration process, but many areas lack runoff data, so it is meaningful to explore how to use these models in these areas. The SWAT model is a process-oriented and physically-based model and is widely recognized as one of the top hydrological models (Alemayehu et al., 2017; Akoko et al., 2021). There are many studies on modelling watersheds using the SWAT model, and remote sensing data are also used to verify the accuracy of the model (Zhang et al., 2021), but there is less research on calibrating the SWAT model using remote sensing data to study ET. Therefore, it is of great significance to study how to make full use of the advantages of remote sensing data and build a hydrological model for ungauged areas to manage regional water resource management. The area studied in this work, the Madu River Basin, is located in the core area of the Three Gorges Reservoir area of China and is adja-

cent to the Shennongjia National Nature Reserve. Water resource monitoring in this region is important for the water ecological security of Shennongjia Nature Reserve and the Three Gorges. The main objectives of this study were: 1) to use a remote sensing ET product to calibrate the SWAT model, 2) to assess the ability of the calibrated SWAT model to simulate ET in the Madu River Basin, and 3) to reveal the spatiotemporal change in ET in the Madu River Basin. In addition, this study explored the potential of remote-sensing-based ET data for hydrological model calibration, which can provide reference for related studies.

2 Materials and Methods

2.1 Study area

The Madu River Basin is in the eastern Chongqing in Central China, which is the core area of the Three Gorges Project (Fig. 1). The region has abundant rainfall and numerous streams and is adjacent to the Shennongjia National Nature Reserve, Hubei Province of China. The Madu River Basin (549.7 km^2) has two main tributaries, the Pingding River and the Miaotang River, which both flow out from Shennongjia Nature Reserve and flow southwest into Wushan County, Chongqing City, where they meet at the Lianghekou outlet in Wushan County to form the Madu River. The river continues to flow westward to the Sancheng Gorge in Wushan County, joins the Daning River, flows into the Yangtze River in Wushan County, and passes through the Three Gorges Dam. The basin is located between 31°11′53″N–31°31′30″N and 109°50′45″E–110°9′25″E, which is a well-protected scenic spot with little influence from human activities and is known as the small Three Gorges. The upstream of the basin is a subalpine basin, where distributed some wetland areas with many peats, which has attracted the attention of many researchers. The topography of the area is undulating. The elevation range is 141–2797 m, which is high in the east and low in the west and is high in upstream, low in downstream and low near the river. The average slope of the basin is 31.03°. The basin has a subtropical monsoon climate with the same periods of rain and heat, and the precipitation and temperature in the vertical direction change significantly and have a significant vertical distribution climate characteristic. The upstream basin is a critical zone (Dajiuhu peatland, Shennongjia Nature Reserve) in which a comprehensive monitoring system has been deployed (Huang et al., 2017). An eddy covariance (EC) tower was set up here (sub-basin No. 1) and provides us with ET measurement data (Weng et al., 2020).

2.2 SWAT model description

A SWAT model was built in this study. The model was described in the literature (Arnold et al., 1998). The

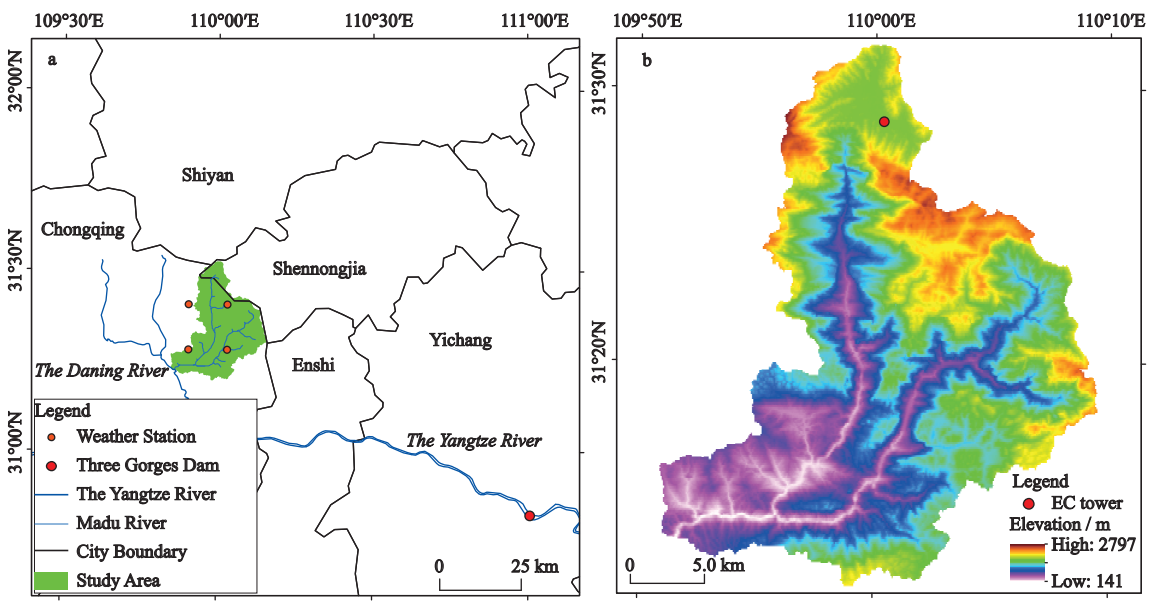

Fig. 1 Geographical and the eddy covariance (EC) tower site locations of the Madu River Basin, central China

SWAT model is a comprehensive and distributed model system. Data about meteorology, soil properties, topography, land-use type, and land management practices in the watershed are necessary to simulate physical processes associated with water movement, sediment movement, crop growth, nutrient cycling, *etc*. (Alemayehu et al., 2017). Based on the powerful spatial processing function of the model, a basin can be partitioned into sub-basins using topographic information and stream networks (Ouessar et al., 2009). Then, these sub-basins are divided into hydrological response units (HRUs), which represent a combination of different land uses, soil types and slope classes. A total of 34 sub-basins and 188 HRUs were delineated in the Madu River Basin. HRUs are the main calculation units of SWAT, where the simulations are controlled by the water balance equation (Neitsch et al., 2009; Sirisena et al., 2020). The water balance is expressed with the following Equation (1):

$$SW_t = SW_0 + \sum_{i=1}^{t}(R_{\text{day}} - Q_{\text{surf}} - E_a - W_{\text{seep}} - Q_{\text{gw}}) \quad (1)$$

where SW_t and SW_0 represent the final and initial soil water contents, respectively, t is the final day, R_{day} is the amount of precipitation on day i, Q_{surf} is the amount of surface runoff on day i, E_a, W_{seep}, and Q_{gw} are the ET, the amount of water entering the vadose zone from the soil profile, and the return flow on day i. All parameters are expressed in mm (Neitsch et al., 2009).

We utilize the actual ET as the fitting variable. Actual ET is calculated in SWAT as the sum of the potential evaporation from the intercept, actual plant transpiration and actual soil water evaporation (Becker et al., 2019). The Penman-Monteith method (Monteith, 1965) was used in SWAT to calculate potential plant transpiration and potential soil water evaporation (Immerzeel and Droogers, 2008; Becker et al., 2019). SWAT calculates reference ET with fixed resistance factors for a reference alfalfa crop and plant type-specific potential ET (ET_p) with varying plant-specific parameters, which are determined by leaf area indices and crop heights. The actual plant transpiration indicates the actual plant water uptake, which is estimated by adjusting ET_p. Actual soil water evaporation is calculated using a soil cover index and available water storage capacity in the soil. All the physical hydrologic processes were computed on a monthly time step during 2008−2018. A daily time step simulation was also carried out during 2017−2018.

2.3 Input data

There are two types of data used for the model. The data and their sources are listed in Table 1. The first type of data includes basic geographic data as follows. 1) Digital elevation model (DEM): a 30 m resolution DEM from the Advanced Spaceborne Thermal Emission and Reflection Radiometer Global Digital Elevation Model Version 2 (ASTER GDEMV2) for the generation of the river network and the sub-basin. 2) Land use: 10 m resolution land cover data from the Finer Resolution Observation and Monitoring of Global Land Cover with 10m resolution (FROM-GLC10) (Gong et al., 2019). 3) Soil database: The soil raster and soil attribute databases were obtained from the Harmonized World Soil Database version 1.1 (HWSD V1.1) (FAO et al., 2009). 4) Slope data: Slope data are calculated from DEM data in ArcGIS. 5) Meteorological data: The China Meteorological Assimilation Driving Datasets for the SWAT model (Version 1.2) (CMADS V1.2) (Meng et al., 2018), which has been widely used in hydrological studies (especially the SWAT model) (Zhang et al., 2020a; Dao et al., 2021; Gao et al., 2021; Zhuang et al., 2021), is used in this study. Its precipitation data were stitched using Climate Prediction Center Morphing Technique (CMORPH)'s global precipitation products and the National Meteorological Information Centre's data of China (which is based on CMORPH's integrated precipitation products). The latter contains daily precipitation records observed at 2400 national meteorological stations and the CMORPH satellite's inversion precipitation products. All these basic geographic data are extracted at the watershed scale. The second type of data includes the following. 1) Remote sensing ET data: the MODIS/Terra Net Evapotranspiration 8-Day L4 Global 500 m SIN Grid (MOD16A2) dataset. This product has released the global evapotranspiration data since 2001, and many basic research or methodological studies have used these data (Zheng et al., 2020; 2021; Ji et al., 2021). 2) Measured ET data derived from the EC tower site. The model behind the MOD16A2 product uses a modified Penman-Monteith approach, which is similar to the method used in the SWAT model, to predict evaporation from wet and dry soil, evaporation from wet canopies, and transpiration from dry canopies (Zhang et al., 2010; Jepsen et al., 2021). The ET in individual

Table 1 Data used in the study

Input data	Format	Details	Source
DEM	Raster	ASTER GDEMV2	GS Cloud
Land use	Raster	FROM-GLC10	THU
Soil	Raster and Microsoft Database	HWSD v1.1	TPDC
Meteorological	Txt	CMADS V1.2	TPDC
ET	Raster	MOD16A2	LAADS DAAC
ET	Txt	EC Tower	SESCUG

Notes: DEM: Digital Elevation Model; ET: evapotranspiration; ASTER GDEMV2: Advanced Spaceborne Thermal Emission and Reflection Radiometer Global Digital Elevation Model Version 2; FROM-GLC10: Finer Resolution Observation and Monitoring of Global Land Cover with 10 m resolution; HWSD v1.1: Harmonized World Soil Database version 1.1; CMADS V1.2: The China Meteorological Assimilation Driving Datasets for the SWAT model (Version 1.2); MOD16A2: MODIS/Terra Net Evapotranspiration 8-Day L4 Global 500 m SIN Grid; EC Tower: Eddy Covariance Tower; GS Cloud: Geospatial Data Cloud, http://www.gscloud.cn/home (Accessed 12 June 2021); THU: Tsinghua University, http://data.ess.tsinghua.edu.cn/fromglc10_2017v01.html (Accessed 12 June 2021); TPDC: National Tibetan Plateau Data Center, http://www.tpdc.ac.cn/zh-hans/. (Accessed 12 June 2021); LAADS DAAC: Level-1 and Atmosphere Archive & Distribution System Distributed Active Archive Center, https://ladsweb.modaps.eosdis.nasa.gov/ (Accessed 12 June 2021); SESCUG: School of Environmental Studies, China University of Geosciences, Wuhan, https://ses.cug.edu.cn/ (Accessed 12 June 2021)

MODIS cells was aggregated to monthly values using time-weighted averaging. Then, the average value of cells in the range is calculated according to the range of each sub-basin.

2.4 Model calibration and validation

Arc-SWAT (Version 2012) was used to set up the model. After the initial SWAT model setup and simulation according to the default parameters, to improve the accuracy of the model, the simulated ET was used as a calibration target in this optimization process. To verify the simulation ability of the model, two core calibration strategies were adopted. The first strategy was lumped calibration (LC), and the second was spatially distributed calibration (SDC). Fourteen parameters related to ET were selected for calibration (Table 2). In LC, to be more representative, we selected seven sub-basins (No. 1, No. 8, No. 12, No. 16, No. 21, No. 24 and No. 25) that are symmetrically distributed along the northeast-southwest direction, occupying the upper, middle, and lower reaches. At the same time, in terms of geographical attributes, this combination includes all land use types, soil types and slope classifications within the study area. Their remote sensing ET was taken as the observation

Table 2 Parameters used in the study

Parameter	Meaning
ALPHA_BF	Baseflow alpha factor / d
GWQMN	Threshold depth of water in the shallow aquifer required for return flow to occur / mm
SOL_AWC (1)	Available water capacity of the first soil layer
GW_REVAP	Groundwater ‘revap’ coefficient
SOL_BD (1)	Moist bulk density of the first soil layer
GW_DELAY	Groundwater delay / d
CH_N2	Manning’s ‘n’ value for the main channel
CH_K2	Effective hydraulic conductivity in main channel alluvium
ALPHA_BNK	Baseflow alpha factor for bank storage
ESCO	Soil evaporation compensation factor
EPCO	Plant uptake compensation factor
HRU_SLP	Average slope steepness
SOL_ALB (1)	Moist soil albedo of the first soil layer
BIOMIX	Biological mixing efficiency

value of the calibration process, and all sub-basins shared the calibrated parameters of the selected sub-basins. In SDC, all sub-basins were calibrated separately. SWAT-CUP (Version 2019, Swiss Federal institute of Aquatic Science and Technology, Swizerland) was used for the calibration. The Sequential uncertainty fitting Version 2 (Sufi-2) algorithm (Abbaspour et al., 2004) was adopted for calibration. The number of simulations for a single calibration was set as 500 times, and multiple iterations were carried out until the best result was achieved. We considered 2008 as the year for the warm-up period, 2009−2014 as the year of model calibration, and 2015−2018 as the year of model validation. Furthermore, the model was verified with remote sensing data during 2015−2016 and verified with measured data from the EC tower site during 2017−2018. The coefficient of determination (R^2) and Nash-Sutcliffe efficiency coefficient (*NSE*) (maximization) (Krause et al., 2005) were used as the objective functions. We also give Root Mean Square Error (*RMSE*) and relative error as part of the accuracy evaluation. The entire flowchart of this optimization process is summarized in Fig. 2.

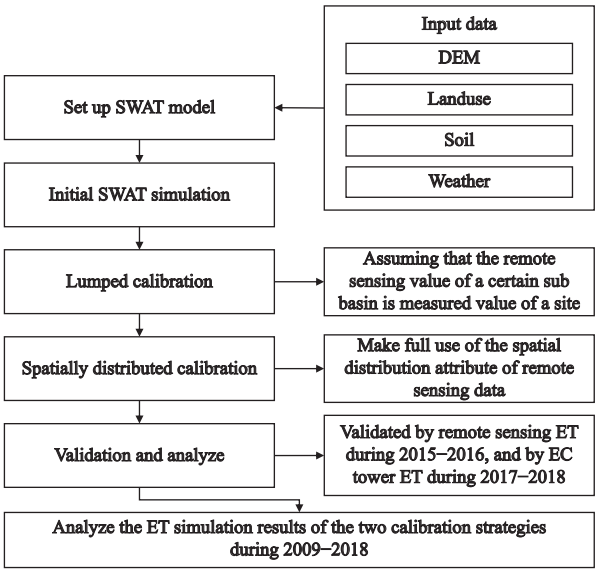

Fig. 2 Flowchart of the SWAT model simulation and optimization process. DEM: Digital Elevation Model; ET: evapotranspiration

3 Results

3.1 Comparison of the validation results

The simulated monthly ET was compared to the ET data derived from the MOD16A2 and EC tower sites. Fig. 3 shows the simulation accuracy after the LC and the SDC. Fig. 3a shows the calculated values of *NSE*, and the values of all 34 sub-basins are greater than 0.6. Fig. 3b shows the calculated value of R^2, and the values of all 34 sub-basins are greater than 0.7. It is believed that when $R^2 > 0.6$ and $NSE > 0.5$, the model simulation results are acceptable (Moriasi et al., 2007). Moreover, the values of *NSE* and R^2 in the validation period are generally higher than those in the calibration period, which is contrary to the general situation. The possible reasons for this unusual result are the distribution of datasets and the basic input data. Overall, the simulation results of the two strategies reasonably met our expectations. In addition, the difference between the R^2 of the two strategies is very small, and the *NSE* of the SDC strategy is significantly higher than that of the LC strategy in both the calibration and validation periods. Fig. 4 shows the relationship between simulated ET and measured ET from 21 October 2017 to 31 August 2018. The accuracy

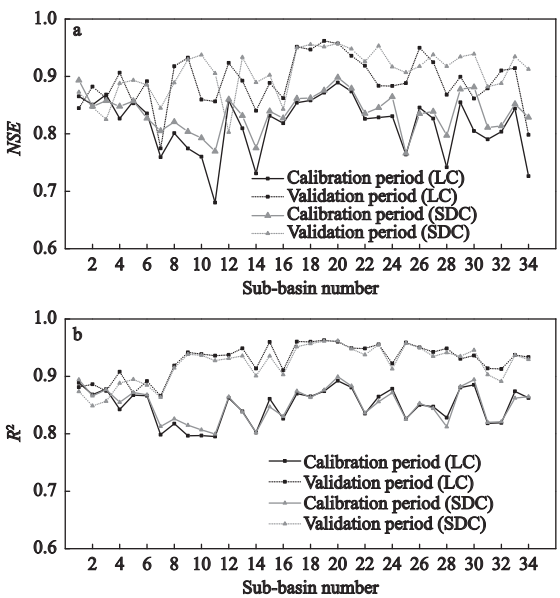

Fig. 3 Accuracy of model simulation of evapotranspiration (ET) in the calibration and validation periods in the Madu River Basin, central China; a. Nash-Sutcliffe efficiency coefficient (*NSE*); b. coefficient of determination (R^2); LC, lumped calibration; SDC, spatially distributed calibration

is good (R^2 = 0.704, *NSE* = 0.759, *RMSE* = 1.97) on a daily time scale, and the simulated ET is generally lower. A possible reason is that through the process of model calibration, the fitting degree between the simulated ET and the remote sensing value is improved, but remote sensing itself is an indirect estimation method, that deviates from the measured value. Overall, the per-

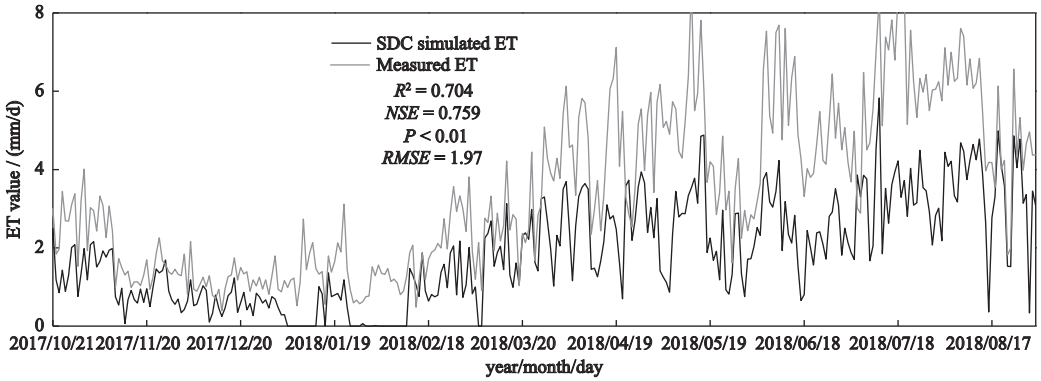

Fig. 4 The relationship between spatially distributed calibration (SDC) simulated evapotranspiration (ET) and measured ET during 2017−2018 in the Madu River Basin, China. R^2, coefficient of determination; *NSE*, Nash-Sutcliffe efficiency coefficient; *RMSE*, Root Mean Square Error

formance of the model is acceptable, and the spatially distributed calibration strategy has the best performance. The simulated monthly ET (SDC) and observed monthly ET are listed in Table S1.

3.2 Comparison of the simulation results

There are several ways to evaluate and compare the simulation accuracy of the two calibration strategies. Fig. 5 shows the monthly and annual scatter plots for the comparison between the simulation results of the two strategies and the remote sensing data at the sub-basin and basin levels. The figure shows that the goodness-of-fit decreases with spatial detail but increases with temporal detail. The R^2 of the monthly basin, for example, is as high as 0.900 (R^2=0.902 (LC), R^2 = 0.900 (SDC)), while at the sub-basin level, the R^2 is nearly 0.860 (R^2 = 0.857 (LC), R^2=0.862 (SDC)). Over time, the patterns observed are not similar. The R^2 at the monthly sub-basin level is higher than 0.8, while the R^2 decreases below 0.5 at the annual sub-basin level, and the same pat-

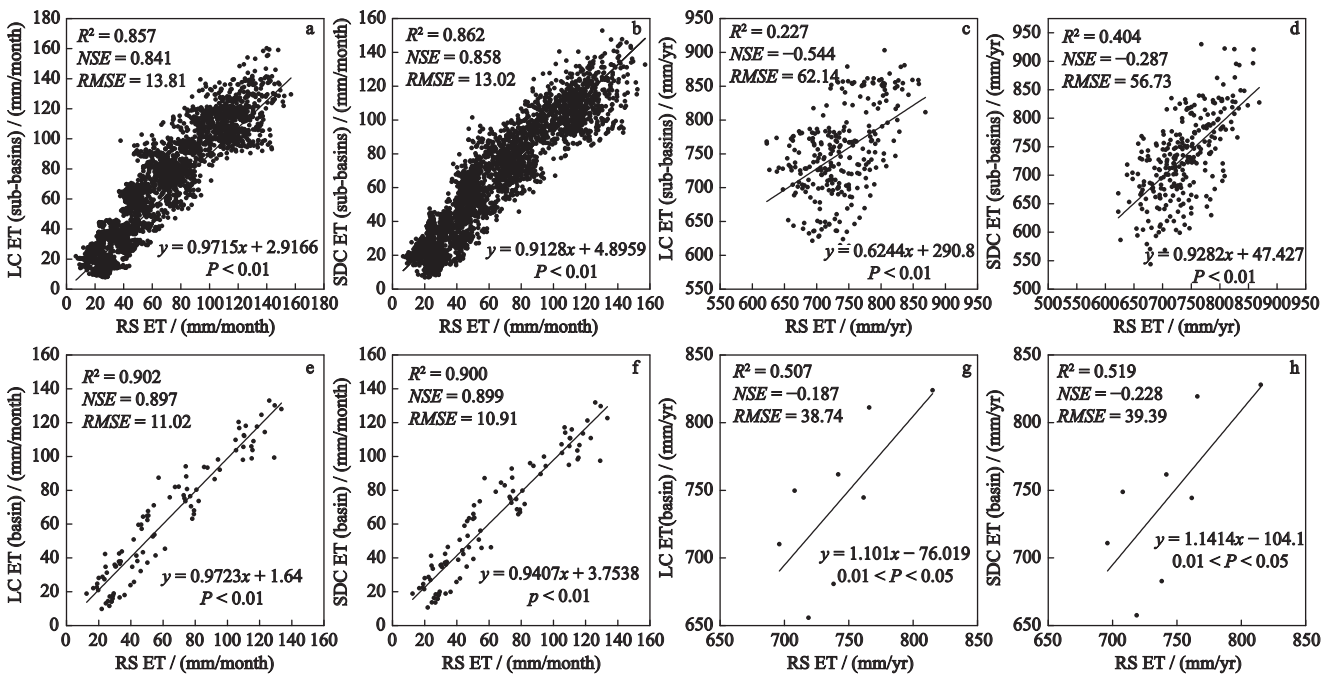

Fig. 5 Comparison of evapotranspiration (ET) simulation accuracy between lumped calibration (LC) and spatially distributed calibration (SDC) in the Madu River Basin, China; a. monthly results of LC (sub-basins); b. monthly results of SDC (sub-basins); c. annual results of LC (sub-basins); d. annual results of SDC (sub-basins); e. monthly results of LC (basin); f. monthly results of SDC (basin); g. annual results of LC (basin); h. annual results of SDC (basin). R^2: coefficient of determination; *NSE*: Nash-Sutcliffe efficiency coefficient; *RMSE*: Root Mean Square Error

tern is also observed at the basin level. Fig. 6 shows the distribution diagram of the value obtained by subtracting the value of remote sensing data from the annual ET obtained by the simulation of all sub-basin during 2009−2016. The LC results have more outliers, and the median is greater than that of SDC, while the SDC results are more evenly distributed. Fig. 7a shows the comparison of the accumulated values of ET obtained by simulation over the years with every sub-basin. Fig. 7b is a clustered bar chart of the value obtained by subtracting the value of remote sensing data from the accumulated values of ET that were obtained by simulation over the years with every sub-basin. The SDC result fits well with the remote sensing data, while the result of LC is only close to the remote sensing data in several sub-basins, and the others do not match or even show the opposite trend. At the basin scale, the sum of ET of 8 yr (2009−2016) of remote sensing data is 5945.26 mm, the result of LC is 5937.82 mm, and the result of SDC is 5953.07 mm.

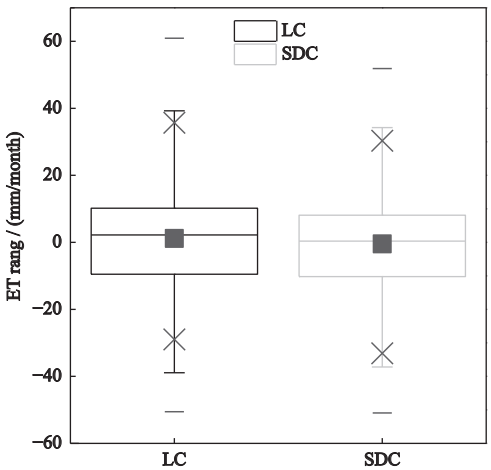

Fig. 6 Box diagram of lumped calibration (LC) and spatially distributed calibration (SDC) evapotranspiration (ET) simulation results (monthly scale) minus remote sensing value in the Madu River Basin, China

3.3 Spatiotemporal change in ET

Based on the simulation results, the spatial and temporal distribution characteristics of ET in the Madu River Basin were analysed. During 2009−2018, the annual average ET of the Madu River Basin was 734.37 mm/yr (SDC results), and ET showed an upwards trend during 2009−2018 (7.21 mm/yr) (Fig. 8a). On a monthly scale, the trends of ET and precipitation with time are similar (Fig. 8b). They are high in summer (June−September, highest in July or August) and are left-right symmetrical unimodal throughout the year, but throughout the year, their highest values do not appear in the same month (except 2010 and 2012). Fig. 9 shows the spatial distribution of ET in the Madu River Basin. Fig. 9a shows the spatial distribution (at sub-basin scale) of the annual average ET during 2009−2018. The No. 3, No. 12, No. 19, and No. 26 sub-basins have the highest annual average ET (approximately 800 mm/yr) while the No. 11, No. 14 and No. 34 have the lowest value (approximately 650 mm/yr), the No. 26 sub-basin has the highest annual average ET (819.31 mm/yr), and the No. 11 sub-basin has the lowest value (625.30 mm/yr). Fig. 9b

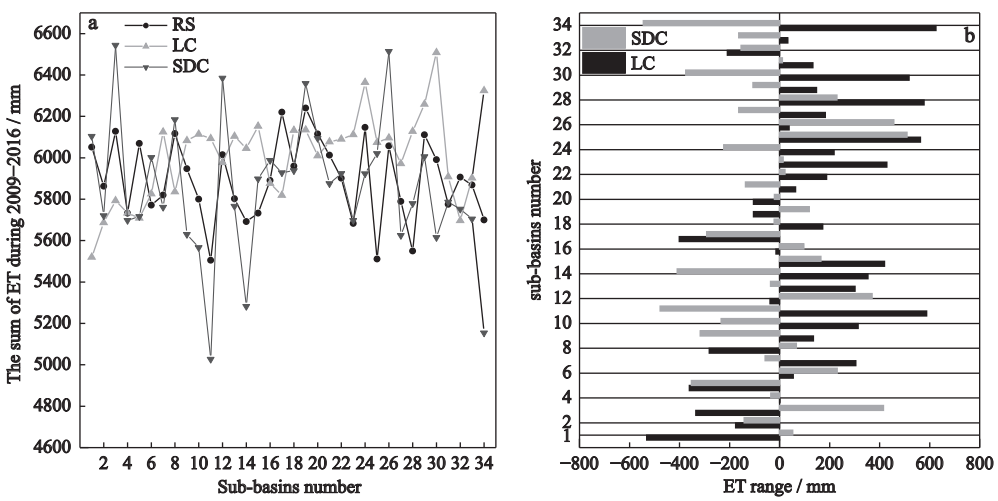

Fig. 7 Comparison of the multiyear evapotranspiration (ET) of spatially distributed calibration (SDC), lumped calibration (LC) and remote sensing products (RS) in each sub-basin of the Madu River Basin, China. a. comparison of multiyear total ET value of each sub-basin; b. multiyear total ET value of each sub-basin simulated by LC and SDC minus the remote sensing value

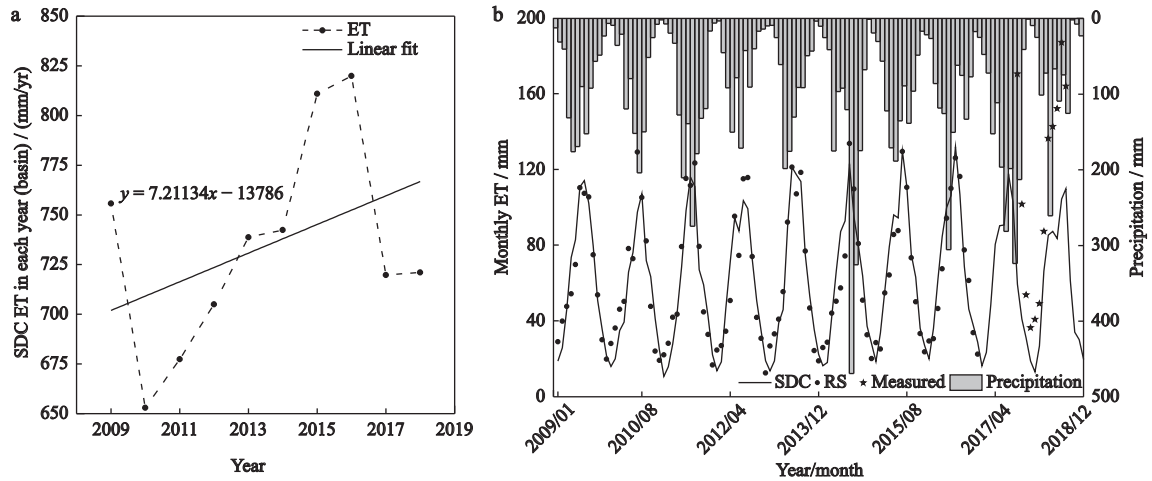

Fig. 8 Variation in evapotranspiration (ET) with time (simulation results of spatially distributed calibration (SDC)) in the Madu River Basin, China; a. interannual variation in ET (basin-scale results of SDC); b. monthly variation in ET (basin-scale results of SDC and remote ET) and precipitation

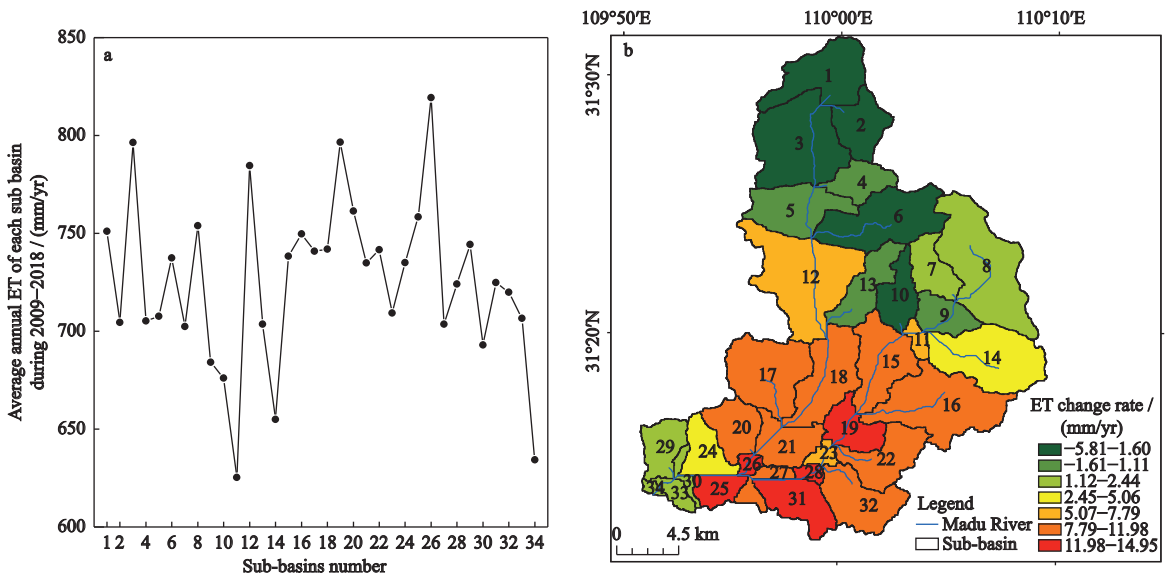

Fig. 9 Spatial distribution of evapotranspiration (ET) during 2009−2018 in the Madu River Basin, China; a. simulated multiyear average ET of each sub-basin; b. annual change rate of ET of each sub-basin

shows the change rate of ET during 2009–2018 (Natural breaks (jenks) method is adopted for change rate classification). Most sub-basins show an upwards trend, and the values of 2009 in all sub-basins are anomalies (they are higher than the values in 2010). The No. 19, No. 25, No. 26, No. 28, and No. 31 sub-basins have the highest change rates, and the sub-basins that are upstream and downstream have the lowest change rates.

3.4 ET-meteorological factors relationships

Considering the incomplete corresponding relationship between ET and precipitation, the results of the linear correlation analysis between monthly and annual ET from SWAT and meteorological factors are listed in Table 3. All meteorological factors are converted to the scale corresponding to ET during the calculation. Precipitation (PCP), average maximum air temperature (T_{max}), average minimum air temperature (T_{min}), relative humidity (RH) and solar radiation (SOR) are positively correlated with monthly ET, while wind speed (WIND) shows no correlation with monthly ET. PCP, SOR and WIND are positively correlated with annual ET, while T_{max}, T_{min}, and RH show no correlation with annual ET.

Table 3 Pearson correlation coefficient (R) between ET and meteorological factors in the Madu River Basin, central China

Factor	PCP	WIND	T_{max}	T_{min}	RH	SOR
Monthly ET	0.678**	0.021	0.945**	0.930**	0.266**	0.808**
Annual ET	0.166	0.626	0.308	0.201	0.034	0.486

Notes: PCP, precipitation; WIND, wind speed; T_{max}, average maximum air temperature; T_{min}, average minimum air temperature; RH, relative humidity; SOR, solar radiation. ** indicates a significance indicates a significance at 0.01; * indicates a significance indicates a significance at 0.05

The correlation between T_{max} and ET is best on the monthly scale, and the correlation between WIND and ET is lowest; however, the correlation between WIND and ET is the best on the annual scale. In fact, when the scale changes from month to year, the correlation of all factors with ET decreases except wind speed, especially for T_{max} and T_{min}. In summary, PCP, T_{max}, T_{min} and SOR were significantly and highly correlated with monthly ET, and SOR, and WIND were moderately correlated with annual ET; in other cases, there was no correlation.

4 Discussion

4.1 Discussion on simulation process and results

The simulation results are encouraging and indicate that the spatially distributed hydrological model SWAT can be successfully calibrated using remotely sensed ET derived from a time series of MODIS images in a poorly gauged area or an ungauged area through two different calibration strategies. Fourteen parameters related to soil, groundwater, runoff, terrain, and vegetation were optimized for a whole basin (LC) or for every sub-basin (SDC). Using monthly remote ET during 2009–2014 as calibration input data, monthly remote ET during 2015–2016 and measured ET data during 2017−2018 derived from the EC tower site as validation data. LC and SDC achieved acceptable simulation results in every sub-basin, and the accuracy of SDC was higher than that of LC. Furthermore, according to the calibrated objective functions—the R^2 and *NSE*—their values in the validation period are even higher than that of the calibration period, which is contrary to the general situation, the possible causes of this unusual result are the uneven temporal distribution of datasets and the difference between the basic input data and the actual situation. The calibration period is one year longer than the verification period, and the verification period is divided into two parts. That is, the distribution of calibrate set and verify set is uneven. In addition, the land use data used in this study is FROM-GLC10, which is a 2017 dataset with a 10 m spatial resolution. Therefore, in the verification period, the land use type of the model is closer to the real situation and the simulation accuracy of the model is better. The results compared with the measured ET also meet the accuracy requirements. In addition, some studies have used other models or other remote sensing ET data to calibrate hydrological models, and the accuracy of the monthly scale we obtained is similar to theirs (Table 4). This shows that the model is applicable in the Madu River Basin. The LC results have more outliers, and the median is greater than that of SDC. Compared with the measured ET, the SDC simulated value is lower, but when compared with the remote sensing data, this underestimation is not obvious, which should be caused by the calibration process. We utilized the maximum fitting degree with the remote sensing data as the calibration goal, but the remote sensing data deviated from the real value as the hydrological variables were indirectly estimated. The monthly and annual scatter plots for the comparison between the simulation results of the two strategies show that the accuracy of the monthly scale simulation

Table 4 Comparison of monthly scale evapotranspiration (ET) simulation accuracy with studies using other remote sensing products

Data sources	ET data	Model	R^2	*NSE*
Parajuli et al., 2018	SEBAL	SWAT	> 0.61	> 0.60
Jin and Jin, 2020	GLEAM	SWAT	> 0.90	> 0.84
This study	MOD16A2	SWAT	> 0.85	> 0.84

Notes: R^2, coefficient of determination; *NSE*, Nash-Sutcliffe efficiency coefficient; SEBAL, Surface Energy Balance Algorithm; GLEAM, Global Land Evaporation Amsterdam Model; MOD16A2, MODIS/Terra Net Evapotranspiration 8-Day L4 Global 500 m SIN Grid; SWAT, Soil and Water Assessment Tool

is higher than that of the annual scale simulation. Relevant study show that the 'Evaporation Paradox' exists in the Dajiuhu Basin (approximately composed of No.1 and No.2 sub-basin) (Wu et al., 2020), that is, the ET of this area does not increase with the increase of temperature, but decreases. During 2009−2018, the annual average ET of the Madu River Basin was 734.37 mm/yr (SDC results), and ET showed an upwards trend during 2009−2018 (7.21 mm/yr). T_{max} and T_{min} were significantly and highly correlated with monthly ET, which may means that the increasing ET originating from increasing temperature (global warming). However, the sub-basins near Shennongjia Nature Reserve that are upstream have a negative ET change rate, which means that ET decreases in these sub-basins, indicating that the 'Evaporation Paradox' also exists in these sub-basins.

4.2 Pros and cons of the two calibration strategies (LC and SDC)

The SDC has several advantages over the LC. First, many basins can not establish flux towers over a large area or even lack flux towers. The SDC itself is more detailed and can effectively use remote sensing ET products in a poorly gauged area or an ungauged area. Moreover, SDC can achieve better model performance when reproducing the spatiotemporal change in ET since the sub-basins are calibrated separately.

We also admit that there are some problems that must be considered. First, compared with LC, the simulation accuracy of SDC is improved, but not by much, especially on the monthly scale of the whole basin (LC: R^2 = 0.902, *NSE* = 0.897; SDC: R^2 = 0.900, *NSE* = 0.899 (Fig.5)). However, although efficiency can be partially improved through parallel computing, distributed calibration occupies more computer resources and has higher requirements for computers. Second, from the perspective of the calibration process, we selected hydrological parameters for the distribution calibration in the calibration process, but sub-basins with different hydrological properties might have quite different sensitive parameters, which means that the calibrated parameters may not be the optimal solution. Each sub-basin may be able to use a set of hydrological parameters independently. This, however, requires a deep understanding of hydrological processes, especially for complex hydrological models with hundreds of parameters such as SWAT (Zhang et al., 2021). If this problem can be solved, the accuracy of SDC should be improved from the perspective of strategy.

We should also see the advantages of LC. Its efficiency is very high, and the results that meet the accuracy requirements can be obtained after fewer calibration times. If there are enough measured values in some sub-basins, we can also refer to LC to select some representative sub-basins and replace the remote sensing values used in the calibration process with the measured values of these sub-basins to achieve a more efficient and representative calibration scheme.

4.3 Limitation

Usually, the parameter calibration of hydrological models uses the measured value of a hydrological flux (such as runoff) (Zhang et al., 2020a; b). Some studies have used remote sensing in the parameterization of hydrological models (Boegh et al., 2004; Kundu et al., 2017; Kittel et al., 2018; Han et al., 2019). Other hydrological variables that can be obtained by remote sensing, such as soil moisture, were not considered in this study.

In addition, the remote sensing data deviate from real values due to their hydrological variables being indirectly estimated. In the calibration process, we assume remote sensing data as observations; for this assumption to make sense, the remote ET would need to be accurate enough to meet the real value; otherwise, the calibration process would only move predictions from the real values to values that more closely match the remote ET (Jepsen et al., 2021). To evaluate the sufficiency of remote ET accuracy, comparing with the measured value is the most reliable method. Such an evaluation was not carried out in this study (we compared simulated ET with measured ET from 21 October 2017 to 31 August 2018, and we think that the amount of measured data can only be used for verification but is not sufficient for improving the accuracy of the model). The study area is in the Three Gorges Reservoir area, and relevant studies in this region show that the MOD16 ET has overall change characteristics that are highly consistent with their results (Zheng et al., 2020).

5 Conclusions

For spatially distributed hydrological models, using remote sensing data as observations is of great signific-

ance for model calibration and application. We simulated ET in the Madu River Basin during 2009−2018 based on the SWAT model calibrated by two different strategies with remote sensing data MOD16A2 as observations and used the measured data during 2017−2018 to verify the accuracy of the model. Our main findings were as follows:

(1) MOD16A2 ET data offer good potential for hydrological model calibration in the study region as the simulation results show a good performance for ET ($R^2 > 0.70$, $NSE > 0.75$ on daily time series (compared with measured ET)).

(2) The SWAT model is applicable in the Madu River Basin, and SDC based on remote sensing data can achieve higher accuracy than LC at all different scales. The simulated ET of SDC is lower than the measured ET.

(3) The annual ET of the whole basin increased over time at a rate of 7.21 mm/yr during 2009−2018. The multiyear average (range) ET was 734.37 mm/yr (653.00–819.95 mm/yr). The annual ET change rate for the sub-basins showed relatively low values upstream and downstream, indicating that the ET in the upstream and downstream regions was more stable. The Sub-basins near Shennongjia Nature Reserve that are upstream have a negative ET change rate, indicating that the 'Evaporation Paradox' also exists in these sub-basins.

(4) Based on the obtained results, the SDC has several advantages over the LC, and such a calibration strategy could lead to better model performance, therefore, when using the spatially distributed hydrological model for regional studies (especially when the study area is poorly gauged area), remote sensing data with spatial distribution should be more utilized in model calibration.

Appendix

Table S1 List of the simulated monthly evapotranspiration (ET) (results of spatially distributed calibration (SDC)) and observed monthly ET in the Madu River Basin, China

Date	Observed value	SDC	Relative error / %	*RMSE* / mm
2009-01	28.98	18.73	35.36	10.91
2009-02	39.84	25.81	35.22	
2009-03	47.57	46.23	2.81	
2009-04	54.26	73.47	35.41	
2009-05	69.76	82.89	18.82	
2009-06	110.29	110.82	0.48	
2009-07	107.36	114.07	6.26	
2009-08	105.44	102.07	3.20	
2009-09	74.91	79.51	6.14	
2009-10	53.66	50.81	5.32	
2009-11	29.96	35.71	19.19	
2009-12	19.74	21.54	9.13	
2010-01	27.98	15.94	43.01	
2010-02	36.18	19.93	44.91	
2010-03	46.11	34.82	24.49	
2010-04	50.28	39.32	21.80	
2010-05	78.21	65.80	15.86	
2010-06	72.84	76.08	4.45	
2010-07	129.11	97.44	24.53	
2010-08	105.12	107.14	1.92	
2010-09	82.16	71.83	12.57	
2010-10	47.62	63.40	33.13	
2010-11	23.98	41.28	72.14	

Continued Table S1

Date	Observed value	SDC	Relative error / %	*RMSE* / mm
2010-12	19.16	24.59	28.31	10.91
2011-01	21.98	10.69	51.37	
2011-02	28.10	15.72	44.06	
2011-03	41.94	27.85	33.60	
2011-04	43.51	44.49	2.24	
2011-05	79.21	68.49	13.54	
2011-06	115.17	98.25	14.69	
2011-07	111.49	115.89	3.95	
2011-08	123.29	110.86	10.08	
2011-09	79.28	67.03	15.46	
2011-10	44.72	59.01	31.95	
2011-11	32.76	42.38	29.37	
2011-12	16.72	22.11	32.25	
2012-01	24.54	13.65	44.38	
2012-02	26.91	18.40	31.63	
2012-03	34.48	46.48	34.82	
2012-04	50.74	71.10	40.13	
2012-05	95.25	94.31	0.99	
2012-06	74.47	87.40	17.36	
2012-07	114.98	103.44	10.04	
2012-08	115.66	99.24	14.20	
2012-09	73.97	72.57	1.88	
2012-10	41.82	50.69	21.19	
2012-11	30.75	34.67	12.73	
2012-12	12.47	18.89	51.51	
2013-01	26.73	13.63	48.99	
2013-02	33.04	18.86	42.92	
2013-03	40.90	38.94	4.81	
2013-04	55.38	45.92	17.09	
2013-05	92.15	89.54	2.83	
2013-06	121.18	121.18	0.00	
2013-07	107.03	117.14	9.45	
2013-08	118.40	113.55	4.10	
2013-09	76.87	74.72	2.80	
2013-10	46.78	53.01	13.32	
2013-11	24.30	35.42	45.76	
2013-12	18.81	22.33	18.70	
2014-01	25.84	16.32	36.85	
2014-02	28.64	17.97	37.27	
2014-03	44.06	42.30	3.99	
2014-04	50.30	65.96	31.15	
2014-05	57.31	87.17	52.08	
2014-06	74.19	92.79	25.07	
2014-07	133.62	122.65	8.21	
2014-08	109.68	94.96	13.42	
2014-09	80.80	79.73	1.33	
2014-10	50.91	63.71	25.14	
2014-11	32.64	37.17	13.86	
2014-12	20.01	28.06	40.18	
2015-01	28.50	18.55	34.91	

Continued Table S1

Date	Observed value	SDC	Relative error / %	*RMSE* / mm
2015-02	25.09	33.58	33.82	10.91
2015-03	54.71	56.05	2.47	
2015-04	64.19	79.13	23.28	
2015-05	85.53	95.98	12.22	
2015-06	87.63	94.36	7.68	
2015-07	129.47	129.72	0.19	
2015-08	110.52	110.75	0.21	
2015-09	73.32	75.02	2.33	
2015-10	50.08	63.04	25.87	
2015-11	33.24	36.10	8.60	
2015-12	23.60	27.04	14.54	
2016-01	29.38	19.97	32.03	
2016-02	30.51	35.98	17.93	
2016-03	46.47	61.75	32.88	
2016-04	67.47	84.44	25.16	
2016-05	94.22	99.83	5.95	
2016-06	109.97	106.14	3.49	
2016-07	126.01	131.89	4.66	
2016-08	116.20	106.64	8.22	
2016-09	77.42	68.67	11.30	
2016-10	61.29	46.22	24.58	
2016-11	33.72	37.65	11.67	
2016-12	22.43	28.74	28.11	
2017-01	–	16.22	–	
2017-02	–	23.30	–	
2017-03	–	48.57	–	
2017-04	–	80.45	–	
2017-05	–	90.27	–	
2017-06	–	90.66	–	
2017-07	–	117.41	–	
2017-08	–	102.85	–	
2017-09	–	59.30	–	
2017-10	–	40.99	–	
2017-11	53.73	30.91	42.48	48.99
2017-12	36.39	18.76	48.44	
2018-01	40.75	12.99	68.13	
2018-02	49.09	26.75	45.51	
2018-03	87.21	66.29	23.98	
2018-04	136.40	85.24	37.50	
2018-05	142.65	87.26	38.83	
2018-06	152.14	83.47	45.14	
2018-07	187.08	104.28	44.26	
2018-08	163.90	109.77	33.03	
2018-09	–	61.29	–	
2018-10	–	34.02	–	
2018-11	–	30.09	–	
2018-12	–	19.62	–	

Note: '–' indicates a lack of data; *RMSE*: Root Mean Square Error

References

Abbaspour K C, Johnson C A, Van Genuchten M T, 2004. Estimating uncertain flow and transport parameters using a sequential uncertainty fitting procedure. *Vadose Zone Journal*, 3(4): 1340–1352. doi: 10.2113/3.4.1340

Akoko G, Le T H, Gomi T et al., 2021. A review of SWAT model application in Africa. *Water*, 13(9): 1313. doi: 10.3390/w13091313

Alemayehu T, Van Griensven A, Woldegiorgis B T et al., 2017. An improved SWAT vegetation growth module and its evaluation for four tropical ecosystems. *Hydrology and Earth System Sciences*, 21(9): 4449–4467. doi: 10.5194/hess-21-4449-2017

Arnold J G, Srinivasan R, Muttiah R S et al., 1998. Large area hydrologic modeling and assessment part I: model development. *Journal of the American Water Resources Association*, 34(1): 73–89. doi: 10.1111/j.1752-1688.1998.tb05961.x

Bastiaanssen W G M, Menenti M, Feddes R A et al., 1998. A remote sensing surface energy balance algorithm for land (SEBAL). 1. Formulation. *Journal of Hydrology*, 212−213: 198−212. doi: 10.1016/S0022-1694(98)00253-4

Becker R, Koppa A, Schulz S et al., 2019. Spatially distributed model calibration of a highly managed hydrological system using remote sensing-derived ET data. *Journal of Hydrology*, 577: 123944. doi: 10.1016/j.jhydrol.2019.123944

Boegh E, Thorsen M, Butts M B et al., 2004. Incorporating remote sensing data in physically based distributed agro-hydrological modelling. *Journal of Hydrology*, 287(1–4): 279–299. doi: 10.1016/j.jhydrol.2003.10.018

Bosshard T, Zappa M, 2008. Regional parameter allocation and predictive uncertainty estimation of a rainfall-runoff model in the poorly gauged Three Gorges Area (PR China). *Physics and Chemistry of the Earth, Parts A/B/C*, 33(17–18): 1095–1104. doi: 10.1016/j.pce.2008.03.004

Bowen I S, 1926. The ratio of heat losses by conduction and by evaporation from any water surface. *Physical Review*, 27(6): 779–787. doi: 10.1103/PhysRev.27.779

Cui Y K, Song L S, Fan W J, 2021. Generation of spatio-temporally continuous evapotranspiration and its components by coupling a two-source energy balance model and a deep neural network over the Heihe River Basin. *Journal of Hydrology*, 597: 126176. doi: 10.1016/j.jhydrol.2021.126176

Dao D M, Lu J Z, Chen X L et al., 2021. Predicting tropical monsoon hydrology using CFSR and CMADS data over the Cau River Basin in Vietnam. *Water*, 13(9): 1314. doi: 10.3390/w13091314

Douna V, Barraza V, Grings F et al., 2021. Towards a remote sensing data based evapotranspiration estimation in Northern Australia using a simple random forest approach. *Journal of Arid Environments*, 191: 104513. doi: 10.1016/j.jaridenv.2021.104513

Dyer A J, 1961. Measurements of evaporation and heat transfer in the lower atmosphere by an automatic eddy-correlation technique. *Quarterly Journal of the Royal Meteorological Society*, 87(373): 401–412. doi: 10.1002/qj.49708737311

FAO (Food and Agriculture Organizatio), IIASA (International Institute for Applied Systems Analysis), ISRIC (International Soil Reference and Information Centre) et al. , 2009. *Harmonized World Soil Database (Vrsion 1.1)*. Rome: Food and Agriculture Organization of the United Nations.

Gao J B, Jiang Y, Anker Y, 2021. Contribution analysis on spatial tradeoff/synergy of Karst soil conservation and water retention for various geomorphological types: geographical detector application. *Ecological Indicators*, 125: 107470. doi: 10.1016/j.ecolind.2021.107470

Gong P, Liu H, Zhang M N et al., 2019. Stable classification with limited sample: transferring a 30-m resolution sample set collected in 2015 to mapping 10-m resolution global land cover in 2017. *Science Bulletin*, 64(6): 370–373. doi: 10.1016/j.scib.2019.03.002

Gui Z L, Liu P, Cheng L et al., 2019. Improving runoff prediction using remotely sensed actual evapotranspiration during rainless periods. *Journal of Hydrologic Engineering*, 24(12): 04019050. doi: 10.1061/(asce)he.1943-5584.0001856

Han P F, Long D, Han Z Y et al., 2019. Improved understanding of snowmelt runoff from the headwaters of China's Yangtze River using remotely sensed snow products and hydrological modeling. *Remote Sensing of Environment*, 224: 44–59. doi: 10.1016/j.rse.2019.01.041

Herman M R, Hernandez-Suarez J S, Nejadhashemi A P et al., 2020. Evaluation of multi- and many-objective optimization techniques to improve the performance of a hydrologic model using evapotranspiration remote-sensing data. *Journal of Hydrologic Engineering*, 25(4): 04020006. doi: 10.1061/(asce)he.1943-5584.0001896

Howell T A, Schneider A D, Jensen M E, 1991. History of lysimeter design and use for evapotranspiration measurements. In: Allen R G (ed). *Lysimeters for Evapotranspiration and Environmental*. New York: American Society of Civil Engineers, 1–9.

Huang Xianyu, Zhang Zhilin, Wang Hongmei et al., 2017. Overview on critical zone observatory at Dajiuhu Peatland, Shennongjia. *Earth Science*, 42(6): 1026–1038. (in Chinese)

Immerzeel W W, Droogers P, 2008. Calibration of a distributed hydrological model based on satellite evapotranspiration. *Journal of Hydrology*, 349: 411–424. doi: 10.1016/j.jhydrol.2007.11.017

Jepsen S M, Harmon T C, Guan B, 2021. Analyzing the suitability of remotely sensed ET for calibrating a watershed model of a mediterranean montane forest. *Remote Sensing*, 13(7): 1258. doi: 10.3390/rs13071258

Ji Y Y, Tang Q Q, Yan L Y et al., 2021. Spatiotemporal variations and influencing factors of terrestrial evapotranspiration and its components during different impoundment periods in the Three Gorges Reservoir area. *Water*, 13(15): 2111. doi: 10.3390/w13152111

Jiang L L, Wu H, Tao J et al., 2020. Satellite-based evapotranspiration in hydrological model calibration. *Remote Sensing*, 12(3): 428. doi: 10.3390/rs12030428

Jin X, Jin Y X, 2020. Calibration of a distributed hydrological model in a data-scarce basin based on GLEAM datasets. *Water*, 12(3): 897. doi: 10.3390/w12030897

Kittel C M M, Nielsen K, Tøttrup C et al., 2018. Informing a hydrological model of the Ogooué with multi-mission remote sensing data. *Hydrology and Earth System Sciences*, 22(2):

1453–1472. doi: 10.5194/hess-22-1453-2018

Krause P, Boyle D P, Bäse F, 2005. Comparison of different efficiency criteria for hydrological model assessment. *Advances in Geosciences*, 5: 89–97. doi: 10.5194/adgeo-5-89-2005

Kundu D, Vervoort R W, van Ogtrop F F, 2017. The value of remotely sensed surface soil moisture for model calibration using SWAT. *Hydrological Processes*, 31(15): 2764–2780. doi: 10.1002/hyp.11219

Li Y, Huang C L, Hou J L et al, 2017. Mapping daily evapotranspiration based on spatiotemporal fusion of ASTER and MODIS images over irrigated agricultural areas in the Heihe River Basin, Northwest China. *Agricultural and Forest Meteorology*, 244–245: 82–97. doi: 10.1016/j.agrformet.2017.05.023

Meng X Y, Wang H, Shi C X et al., 2018. Establishment and evaluation of the China meteorological assimilation driving datasets for the SWAT model (CMADS). *Water*, 10(11): 1555. doi: 10.3390/w10111555

Monteith J L, 1965. Evaporation and environment. *Symposia of the Society for Experimental Biology*, 19: 205–234.

Moriasi D N, Arnold J G, Van Liew M W et al., 2007. Model evaluation guidelines for systematic quantification of accuracy in watershed simulations. *Transactions of the ASABE*, 50(3): 885–900. doi: 10.13031/2013.23153

Mu Q Z, Heinsch F A, Zhao M S et al., 2007. Development of a global evapotranspiration algorithm based on MODIS and global meteorology data. *Remote Sensing of Environment*, 111(4): 519–536. doi: 10.1016/j.rse.2007.04.015

Mu Q Z, Zhao M S, Running S W, 2011. Improvements to a MODIS global terrestrial evapotranspiration algorithm. *Remote Sensing of Environment*, 115(8): 1781–1800. doi: 10.1016/j.rse.2011.02.019

Neitsch S L, Arnold J G, Kiniry J R et al, 2009. *Soil & Water Assessment Tool Theoretical Documentation Version 2009*. Texas: Texas Water Resources Institute, 1–618

Newman B D, Wilcox B P, Archer S R et al., 2006. Ecohydrology of water-limited environments: a scientific vision. *Water Resources Research*, 42(6): W06302. doi: 10.1029/2005WR004141

Ouessar M, Bruggeman A, Abdelli F et al., 2009. Modelling water-harvesting systems in the arid south of Tunisia using SWAT. *Hydrology and Earth System Sciences*, 13(10): 2003–2021. doi: 10.5194/hess-13-2003-2009

Parajuli P B, Jayakody P, Ouyang Y, 2018. Evaluation of using remote sensing evapotranspiration data in SWAT. *Water Resources Management*, 32(3): 985–996. doi: 10.1007/s11269-017-1850-z

Sirisena T A J G, Maskey S, Ranasinghe R, 2020. Hydrological model calibration with streamflow and remote sensing based evapotranspiration data in a data poor basin. *Remote Sensing*, 12(22): 3768. doi: 10.3390/rs12223768

Sivapalan M, Takeuchi K, Franks S W et al., 2003. IAHS decade on predictions in ungauged basins (PUB), 2003–2012: shaping an exciting future for the hydrological sciences. *Hydrological Sciences Journal*, 48(6): 857–880. doi: 10.1623/hysj.48.6.857.51421

Wang Y Y, Horton R, Xue X Z et al., 2021. Partitioning evapotranspiration by measuring soil water evaporation with heat-pulse sensors and plant transpiration with sap flow gauges. *Agricultural Water Management*, 252: 106883. doi: 10.1016/j.agwat.2021.106883

Weng Wenchang, Ge Jiwen, Chen Jiawei et al., 2020. Water vapor flux characteristics and their relationship with environmental factors in the subalpine peat wetlands of Dajiuhu, Shennongjia. *Plant Science Journal*, 38(4): 493–505. (in Chinese)

Wu Zongfan, Zhang Lihua, Liu Dandan et al., 2020. Simulation of evapotranspiration based on BEPS-TerrainLab V2.0 from 1990 to 2018 in the Dajiuhu Basin. *Chinese Geographical Science*, 30(6): 1095–1110. doi: 10.1007/s11769-020-1160-x

Xu T R, Guo Z X, Xia Y L et al., 2019. Evaluation of twelve evapotranspiration products from machine learning, remote sensing and land surface models over conterminous United States. *Journal of Hydrology*, 578: 124105. doi: 10.1016/j.jhydrol.2019.124105

Zeng Z Z, Piao S, Lin X et al., 2012. Global evapotranspiration over the past three decades: estimation based on the water balance equation combined with empirical models. *Environmental Research Letters*, 7(1): 014026. doi: 10.1088/1748-9326/7/1/014026

Zhang D D, Tan M L, Dawood S R S et al., 2020a. Comparison of NCEP-CFSR and CMADS for hydrological modelling using swat in the Muda River Basin, Malaysia. *Water*, 12(11): 3288. doi: 10.3390/w12113288

Zhang K, Kimball J S, Nemani R R et al., 2010. A continuous satellite-derived global record of land surface evapotranspiration from 1983 to 2006. *Water Resources Research*, 46(9): W09522. doi: 10.1029/2009WR008800

Zhang L, Zhao Y B, Ma Q M et al., 2021. A parallel computing-based and spatially stepwise strategy for constraining a semi-distributed hydrological model with streamflow observations and satellite-based evapotranspiration. *Journal of Hydrology*, 599: 126359. doi: 10.1016/j.jhydrol.2021.126359

Zhang L M, Meng X Y, Wang H et al., 2020b. Investigate the applicability of CMADS and CFSR reanalysis in Northeast China. *Water*, 12(4): 996. doi: 10.3390/W12040996

Zhang Y Q, Chiew F H S, Liu C M et al., 2020c. Can remotely sensed actual evapotranspiration facilitate hydrological prediction in ungauged regions without runoff calibration? *Water Resources Research*, 56(1): e2019WR026236. doi: 10.1029/2019WR026236

Zheng Y H, Wang L S, Chen C et al., 2020. Using satellite gravity and hydrological data to estimate changes in evapotranspiration induced by water storage fluctuations in the Three Gorges Reservoir of China. *Remote Sensing*, 12(13): 2143. doi: 10.3390/rs12132143

Zheng Y H, Wang L S, Fu Z Y et al., 2021. Using GRACE and hydrological data to estimate changes of evapotranspiration in the Three Gorges Reservoir. *IOP Conference Series:Earth and Environmental Science*, 660(1): 012093. doi: 10.1088/1755-1315/660/1/012093

Zhuang Q F, Shi Y T, Shao H et al., 2021. Evaluating the SSEBop and RSPMPT models for irrigated fields daily evapotranspiration mapping with MODIS and CMADS data. *Agriculture*, 11(5): 424. doi: 10.3390/agriculture11050424